

## Hyperspectral Remote Sensing in Characterizing Soil Salinity Severity using SVM Technique: A Case Study of Iraqi Alluvial Plain

Amal Muhammad Saleh

College of Agriculture /University of Baghdad  
[mhmmd1961@aol.com](mailto:mhmmd1961@aol.com)

**Abstract:** Hyperspectral remote sensing is a promising tool for analysing and evaluating the risk of increasing soil salinity especially in arid and semiarid areas. It either occurs naturally or is human-induced. The aim of this paper was to introduce an attempt for monitoring and mapping soil salinity using hyperion data in the capital of Iraq/Baghdad. The Modified Soil Adjusted Vegetation Index (MSAVI<sub>2</sub>), Normalized Difference Water Index (NDWI), Desertification Soil Index (DSI), and Salinity Index (SI) were chosen as evaluation factors for characterizing and mapping soil salinity severity. The extent of salt-affected soils of the study area was divided into four classes: Slightly Saline, Saline, Strongly Saline, and Extremely Saline. The results indicated that Support Vector Machine (SVM) technique generated soil salinity map with overall classification accuracy of 88.33% percent, and with a kappa statistic of 0.8444. Application of this technique showed high accuracy for mapping soil salinity severity using various indices generated from hyperspectral remote sensing data. It is concluded that these hyperspectral indices can be used to detect soil salinity effectively and the SVM algorithm is an efficient method for mapping and assessment soil salinity.

[Amal Muhammad Saleh. **Hyperspectral Remote Sensing in Characterizing Soil Salinity Severity using SVM Technique: A Case Study of Iraqi Alluvial Plain.** *J Am Sci* 2017;13(11):47-64]. ISSN 1545-1003 (print); ISSN 2375-7264 (online). <http://www.jofamericanscience.org>. 6. doi:[10.7537/marsjas131117.06](https://doi.org/10.7537/marsjas131117.06).

**Keywords:** hyperion hyperspectral indices; salt salinity severity; support vector machine (SVM); salinity index.

### 1. Introduction

A soil is said to be saline if the electrical conductivity of its saturation extract (EC<sub>e</sub>) is greater than 4 dS m<sup>-1</sup> (decisiemens per meter). Saline soils contain excess soluble salts, generally chlorides and sulfates, with some carbonates and bicarbonates, of sodium, potassium, calcium, and magnesium. Soil salinity is harmful for plants barring the halophytes; it causes water stress through osmotic disturbances in plant tissue and by toxicity of some salt constituents. Some soils are naturally saline. They are formed by processes called primary salinization or natural salinization. Some soils are made saline by mismanagement of soil and crop, particularly improper irrigation and drainage, that is, changing the hydrologic balance. This is known as secondary salinization or human-induced salinization. Salinization, both natural and human induced, may occur in two climatic settings – arid and semiarid and humid regions. In arid and semiarid regions, scarcity of water due to low rainfall and high evaporation does not allow necessary leaching of salts. Moreover, there is a net capillary rise of water which brings salts to the surface soil. In humid areas, on the other hand, excess irrigation or poor drainage cause the groundwater table to rise to the root zone of plants and make the soil saline (Khan, 2014).

Surface reflectance is highly affected by soil's moisture content, salt content, color, and surface roughness. High salt concentrations can be identified

through the existence of characteristic vegetation types and growth patterns or by the salt efflorescence and crust that are present on bare soils. Researchers have developed different salinity indices to detect and map soil salinity. Remote sensing data have been used extensively to identify and map saline areas, and the potential of remote sensing for assessing and mapping soil salinity is enormous. Multispectral satellite sensors are the preferred method for mapping and monitoring soil salinity, largely due to the low cost of such imagery and the ability to map extreme surface expressions of salinity. However, multispectral data have limited capabilities due to their spatial and spectral resolution. Hyperspectral imagery, with its fine spatial and spectral resolutions, allows soil salinity mapping in greater detail and represents another alternative (Allbed and Kumar, 2013).

Use Support Vector Machine to perform supervised classification on images using a support vector machine (SVM) to identify the class associated with each pixel. SVM provides good classification results from complex and noisy data. SVM is a classification system derived from statistical learning theory. It separates the classes with a decision surface that maximizes the margin between the classes. The surface is often called the optimal hyperplane, and the data points closest to the hyperplane are called support vectors. The support vectors are the critical elements of the training set. The advantages of (SVM) are: (1) effective in high dimensional spaces; (2) still effective

in cases where number of dimensions is greater than the number of samples; (3) uses a subset of training points in the decision function (called support vectors), so it is also memory efficient (Wu et al., 2004).

The present study was undertaken with the objective of mapping soil salinity severity of the capital of Iraq / Baghdad using SVM technique.

## 2. Material and Methods

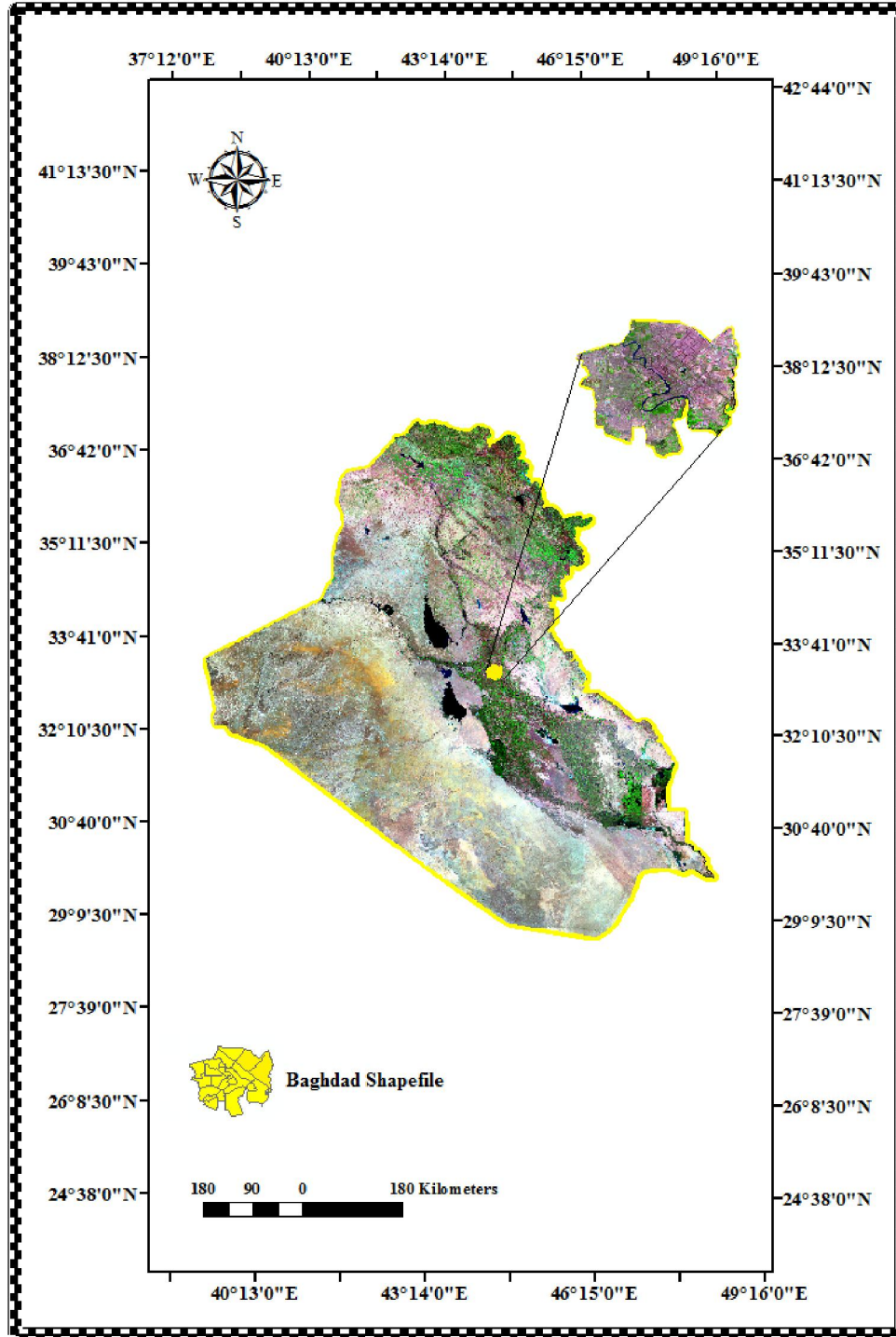


Figure 1. Location map of the study area.

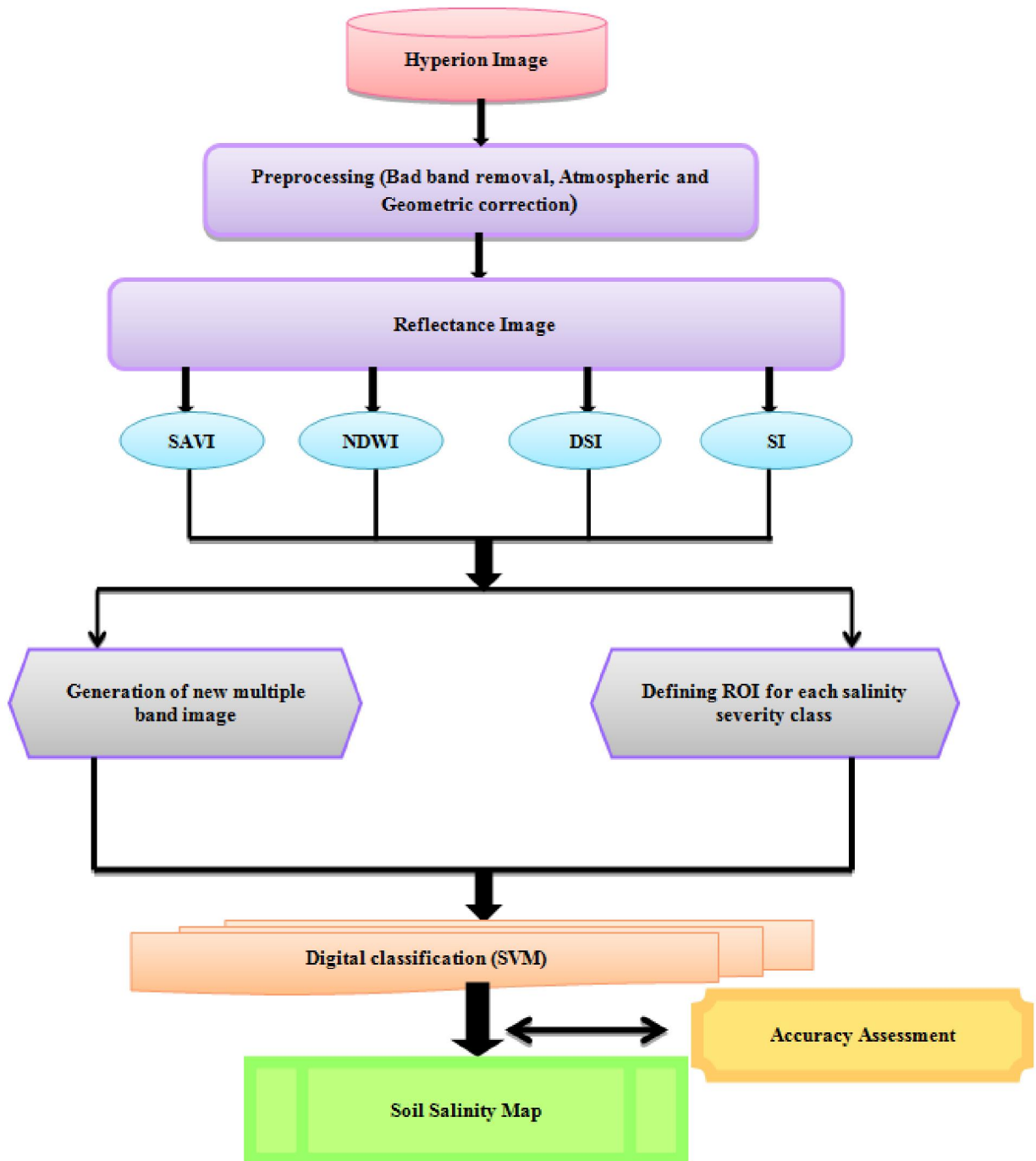


Figure 2. Brief methodology adopted in the study.

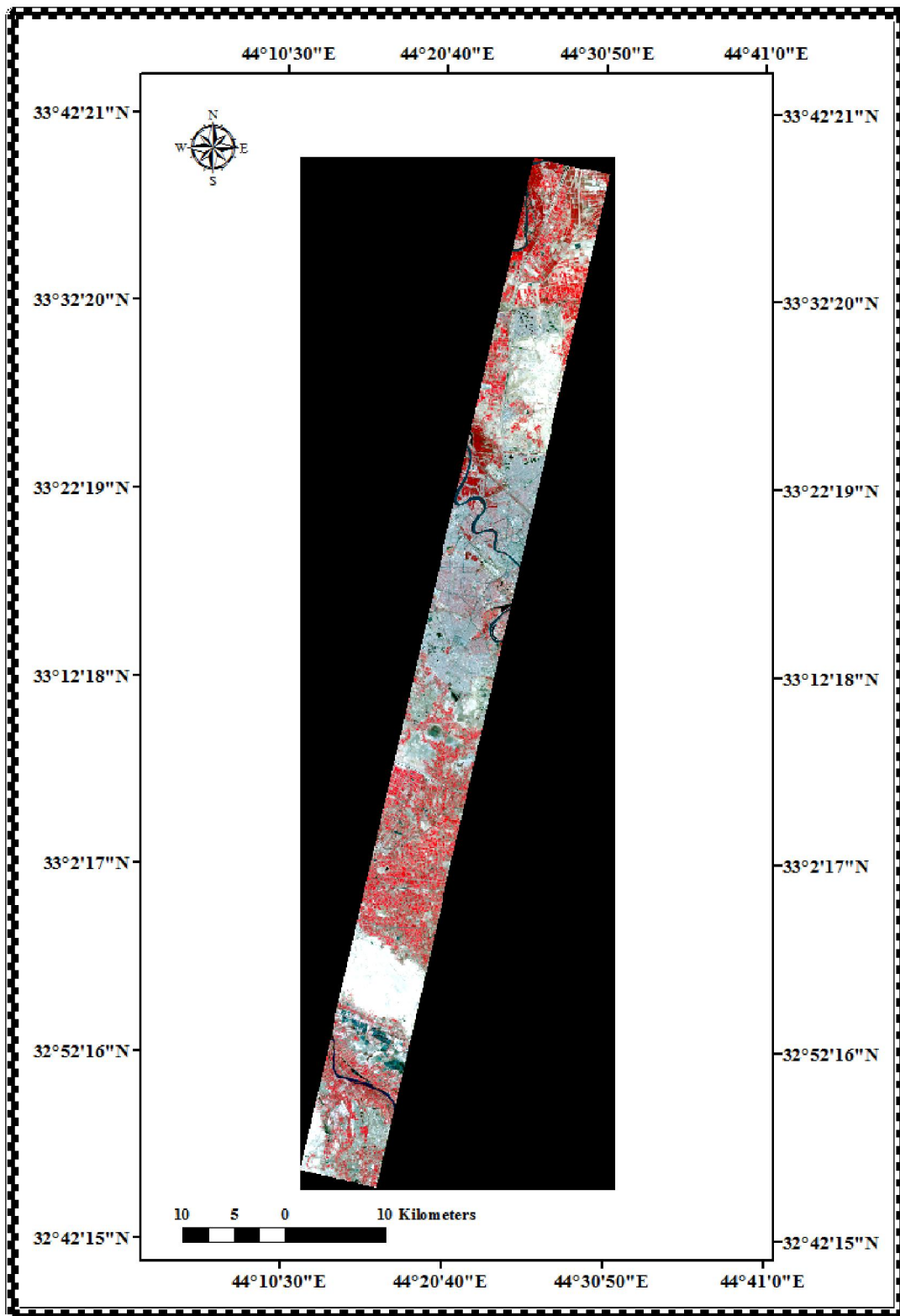


Figure 3. Hyperion data of the study area.

Baghdad is the capital of the Republic of Iraq. The city is located on a vast plain bisected by the River Tigris. The Tigris splits Baghdad in half, with the eastern half being called 'Risafa' and the Western half known as 'Karkh'. The land on which the city is built is almost entirely flat and low-lying, being of alluvial origin due to the periodic large floods which have occurred on the river. It is geographically situated on latitude 33° 18' 46.0980" North and longitude 44° 21' 41.3568" East (Fig. 1).

Baghdad has a subtropical desert climate (Köppen climate classification BWh) and is one of the hottest cities in the world. In the summer from June to August, the average maximum temperature is as high as 44 °C (111 °F) accompanied by blazing sunshine. Rainfall has in fact been recorded on fewer than half a dozen occasions at this time of year and has never exceeded 1 millimetre (0.04 in). The humidity is typically very low (under 10%) due to Baghdad's distance from the marshy southern Iraq and the coasts of Persian Gulf, and dust storms from the deserts to the west are a normal occurrence during the summer. Winters boast mild days and chilly nights, the average January low is 3.8 °C (38.8 °F) but lows below freezing only occur a couple of times per year. Annual rainfall, almost entirely confined to the period from November to March, averages around 150 mm (5.91 in), but has been as high as 338 mm (13.31 in) (Brugge, 2014). The brief methodology adopted for our study is shown in Fig. (2).

Hyperion data were acquired over Baghdad city on 7-April, 2005 at 07:23:41 UTC (Fig. 3). The EO-1 satellite is in a sun-synchronous orbit at 705 km altitude. Hyperion images 256 pixels with a nominal size of 30 m on the ground over a 7.65 km swath (Table 1). Hyperion data is acquired in pushbroom mode with two spectrometers. One operates in the VNIR range (70 bands between 356-1058 nm with an average FWHM of 10.90 nm) and the other in the SWIR range (172 bands between 852- 2577 nm, with an average FWHM of 10.14 nm). Of the 242 Level L1R bands, 44 are set to zero by software during Level L1R processing (bands 1-7, 58-76, 225-242).

Post-Level L1R data processing of the acquired Hyperion scene contains correction for striping pixels, FLAASH atmospheric correction, and Geometric Correction. Hyperion data includes digital number to radiance transformation, radiance to reflectance conversion as described in this section.

The first 12 VNIR bands and many SWIR bands of Hyperion are influenced by striping. Using the ENVI 5.1 remote sensing software package, the

abnormal pixels' DN values are replaced with the average DN values of the immediate left and right neighboring pixels, assuming that nearby pixels have the highest spatial autocorrelation with a center pixel (Goodenough et al., 2003). The abnormal pixel detection algorithm performed well for most bands, except for intensively striped ones.

The nature of remote sensing requires that solar radiation pass through the atmosphere before it is collected by the instrument. Because of this, remotely sensed images include information about the atmosphere and the earth's surface. For those interested in quantitative analysis of surface reflectance, removing the influence of the atmosphere is a critical pre-processing step. To compensate for atmospheric effects, properties such as the amount of water vapor, distribution of aerosols, and scene visibility must be known. Atmospheric and radiometric corrections were performed using the ENVI 5.1 remote sensing software package using FLAASH atmospheric correction modeling tool that corrects wavelengths in the visible through near-infrared and shortwave infrared regions, up to 3µm (ENVI, 2009) (Fig. 4). The various parameters used in FLAASH atmospheric correction are given in Table (2).

**Table 1. Summary of Hyperion Sensor (EO-1) characteristics.**

Parameters	Hyperspectral - EO-1
EO-1 launched	21 November 2000
Altitude	705 km
Swath Width	7.5 km
Spatial Resolution	30 m
Spectral Resolution	10 nm
Radiometric resolution	12 bits
Spectral Coverage	Continuous
Pan Band Resolution	N/A
Spectral channels	220 unique channels
VNIR range	70 channels, 356-1058 nm
SWIR range	172 channels, 852-2577 nm
No. of columns	3400
No. of lines	256

[Source: Liao et al., 2000]



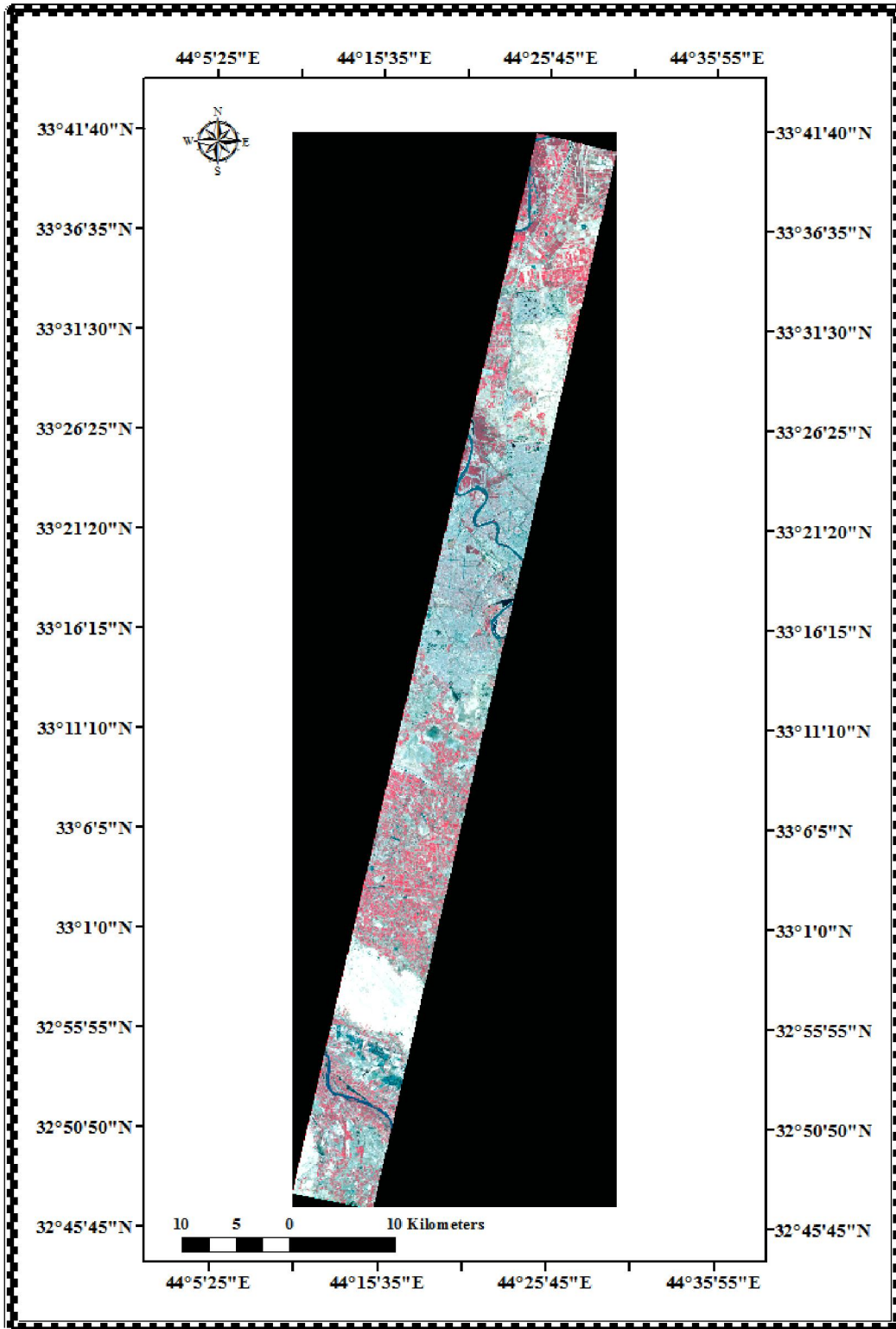


Figure 5. Geometric corrected image of the study area.

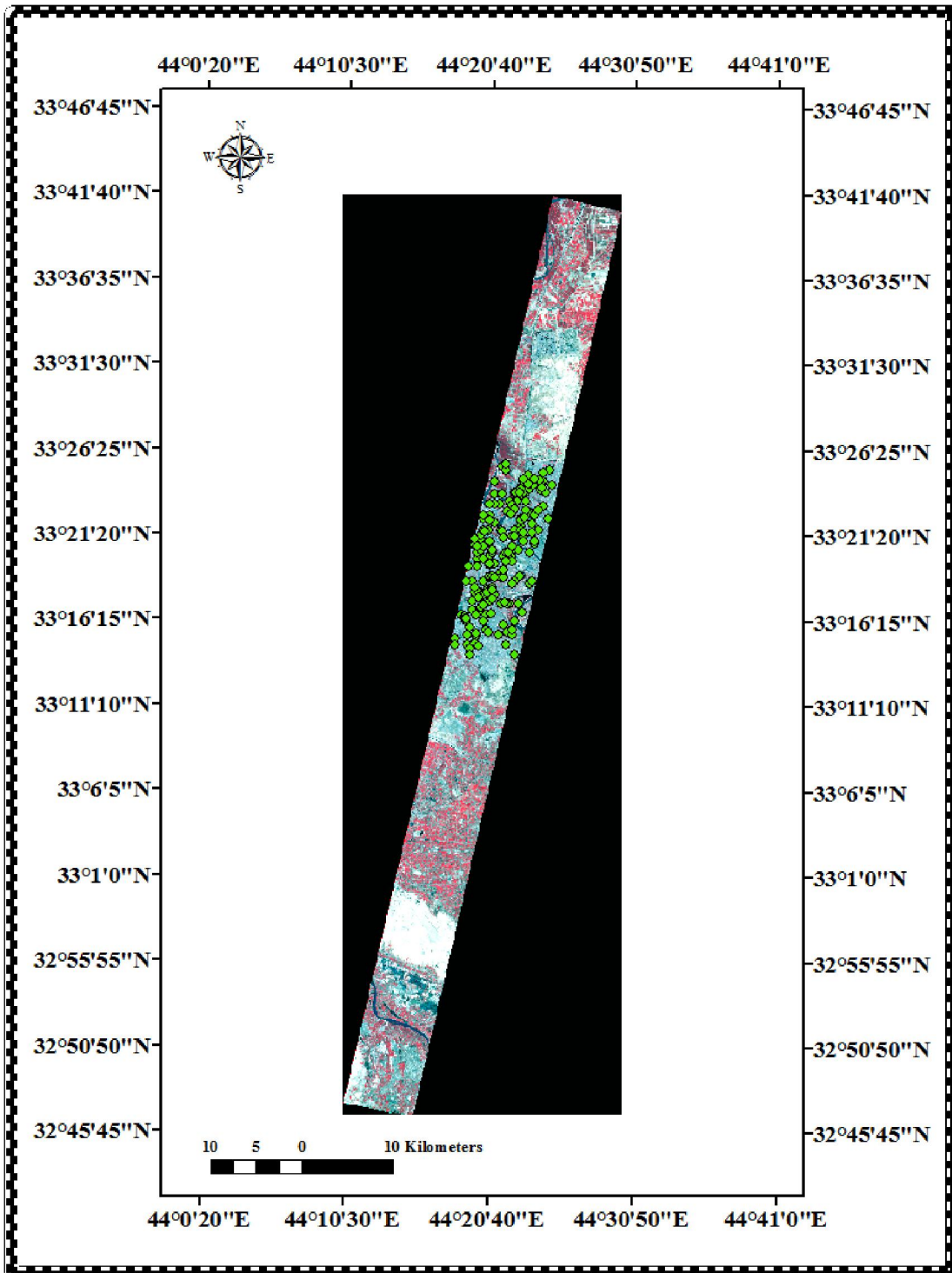


Figure 6. Image of the study area with soil sampling points.

**Table 3. Chemical-Physio characteristics of the study area.**

No. of Samples	ECe dSm <sup>-1</sup>	Classification	Texture
45	< 4	Slightly Saline	Loam

**Table 4. Vegetation and soil indices used in this study.**

Spectral Indices	Equation	Reference
Modified Soil Adjusted Vegetation Index	$MSAVI_2 = \frac{(2 * R_{864nm} + 1 - \sqrt{(2 * R_{864nm} + 1)^2 - 8 * (R_{864nm} - R_{660nm})})}{2}$	Qi et al. (1994)

The geometric correction was carried out in relation to the 1:50000 topographic map covering the study area using a polynomial approach. The correction accuracy was determined by calculating the residual errors between the value obtained by the application of the function and the actual value (Fig. 5).

Hyperion data consists of number of continuous spectral bands, each pixel of which stored the energy as a digital number (DN). The digital numbers were stored as 16-bit signed integer. The following equation was used on individual band to convert DN into Radiance values. Each band of VNIR (1 to 70) and SWIR (71 to 242) was divided by its scale factor i.e 40 and 80 respectively (Thenkabail et al., 2004a).

$$\frac{VNIR}{40}, \frac{SWIR}{80}$$

To convert the radiance into reflectance, following formula was used on individual band and was stacked in further processing steps (ThenkabailPS,2004b):

$$\rho_p = \frac{\pi L_\lambda d^2}{ESUN_\lambda \cos \theta_s}$$

Where:

$\rho_p$  = Unitless planetary reflectance.

$L_\lambda$  = Spectral radiance at the sensor's aperture.

$d^2$  = Earth-Sun distance in Astronomical units.

$ESUN_\lambda$  = Mean solar exoatmospheric irradiances.

$\theta_s$  = Solar zenith angle in degrees.

Earth-sun distance was calculated using following equation:

$$d = 1 - 0.01672 * \cos(0.9856 * (\text{Julian Day} - 4))$$

A total number of 180 random soil samples at depths of 0-30 cm were collected by Ministry of Water Resources/National Center for Water Resources in April and March-2005, hence the dataset was possible to evaluate the soil salinity conditions. Each sampling site was georeferenced and located on the ground by the use of a GPS into UTM projection (Zone 38 North, WGS 84) (Fig. 6). The standard procedure of determining soil extract salinity in terms of Electrical Conductivity (EC) was followed according to Shaw (1994) under laboratory condition (Table 3).

Table (4) summarize vegetation and soil indices that have been proposed and used for soil salinity monitoring and mapping in this study.

Salt affected soils are usually characterized by poorly vegetated developed areas and such state of stressed vegetation could be an indirect indicator to predict and map soil salinity. Among the vegetation indices, A Modified Soil Adjusted Vegetation Index (MSAVI<sub>2</sub>) was used in current study.

The Normalized Difference Water Index (NDWI) is a satellite-derived index from the Near-Infrared (NIR) and Short Wave Infrared (SWIR) reflectance which makes it sensitive to changes in liquid water content and in spongy mesophyll of vegetation canopies (Gao, 1996).

Desertification through soil salinization as a process of land degradation is active in arid and semi-arid environment. Concerning the data required for estimating the Environmental Sensitivity to desertification, the Desertification Soil Index (DSI) was computed. The reflective difference between

1648 nm and 498 nm can highlight the desertification soil (Wu et al., 2010).

The assessment of soil salinity was worked using Soil Salinity Index (SI). This index was obtained depending on the factors related to the parent material (PM), the electrical conductivity of soils (EC), drainage (D) and to the field slope (S). The data recorded in the red spectral band were used in the analysis to check an idea to use just spectral satellite data in this band for salt-affected area delineation (Khan et al., 2001).

Support Vector Machine a classification system derived from statistical learning theory. It separates the classes with a decision surface that maximizes the margin between the classes. The surface is often called the optimal hyperplane, and the data points closest to the hyperplane are called support vectors. The support vectors are the critical elements of the training set. SVM includes a penalty parameter that allows a certain degree of misclassification, which is particularly important for non-separable training sets. The ENVI SVM classifier provides four types of kernels: linear, polynomial, radial basis function (RBF), and sigmoid. The default is the radial basis function kernel, which works well in most cases.

$$\mathbf{RBF} K(\mathbf{x}_i, \mathbf{x}_j) = \exp(-g\|\mathbf{x}_i - \mathbf{x}_j\|^2), g > 0$$

Where:

$K(\mathbf{x}_i, \mathbf{x}_j)$  is called kernel function;  $\mathbf{x}_i$  and  $\mathbf{x}_j$  are training vectors.

$g$  is the gamma term in the kernel function.

SVM examines all of the rule image values to determine those that exceed the reclassification probability threshold. The class information and probability information associated with these pixels are stored for later application to the result image. The examination process continues at the next higher-resolution pyramid level, except that SVM performs classification only for pixels that are not marked as classified at the lower-level resolution. The process repeats until it reaches the full-resolution layer (Hsu et al., 2007).

### 3. Results

Soil salinity index as a remotely sensed indicator, typically depends on the vegetation growing conditions which are helpful for mapping spatially the distribution of soil salinity (Tilley et al., 2007). According to Carter (1993) cell structure damage and chlorophyll reduction could be reliably measured using reduced near infrared reflectance (NIR) and increased visible reflectance (VIS) among several plant species in response to stress. The resulting MSAVI<sub>2</sub> values in the classified image are either

positive, negative or zero. A positive MSAVI<sub>2</sub> value indicates that there is an increase in the vegetation, while a negative value indicates a decrease in vegetation. A zero value indicates no change in vegetation. As halophytic vegetation grows naturally in saline soils, therefore, it has been used as an indirect indicator to predict and map soil salinity (Allbed and Kumar 2013). Fig. (7) showed MSAVI<sub>2</sub> values for the whole study area with a maximum value of 0.404 and a minimum value of 0.886 indicating the influence of salinity on vegetation.

The Normalized Difference Water Index was proposed for remote sensing of vegetation liquid water from space. Absorption by vegetation liquid water near 860  $\mu\text{m}$  was negligible. Weak liquid absorption at 1240  $\mu\text{m}$  was present (Gao, 1996). Spatial distribution of NDWI index was mapped (Fig. 8) with a maximum value of 0.710 and a minimum value of 1.324 indicating that salinity increases with lower NDWI values which explained due to salt accumulation in soils. Under salinity stress conditions, there is no enough available water in soils for proper vegetation growth (Yang et al., 2011).

The Desertification Soil Index for assessing and mapping of desertification was adopted for investigating the active desertification processes in this study area depending upon the soils, climate, vegetation and soil management. Wu, et al. (2010) reported that in DSI imagery, the desertification soil has the highest DSI value (bright), the bare land, wild grass ground and cultivated land have relatively high values (middle) while the vegetation and water bodies had low values (dark). Fig. (9) shows the spatial distribution of DSI index in the study area indicating that the high sensitive areas for desertification may be due to the poor vegetation cover, and human factors. The low sensitivity for desertification is due to the good vegetation cover and soil quality.

The study area consisted to be the area of extreme temperature ranges. Excess irrigation regimes in poor drain soils lead to waterlogging problems and salts accumulation (Elhag, 2016). Singh and Sirohi (1994) noted that a crusted saline soil surface is generally smoother than a non-saline surface and exhibits high reflectance in the visible and NIR bands. Despite the effects of salt features on the soil surface on the spectral reflectance, they have been considered good direct indicators of soil salinity. ( Fernandez-Buces et al., 2006). Estimated values of Soil Salinity Index was used to map and classify soil salinity in the whole study area indicating that the vegetation as well as waterlogged areas are having the least values for salinity index (Fig 10).

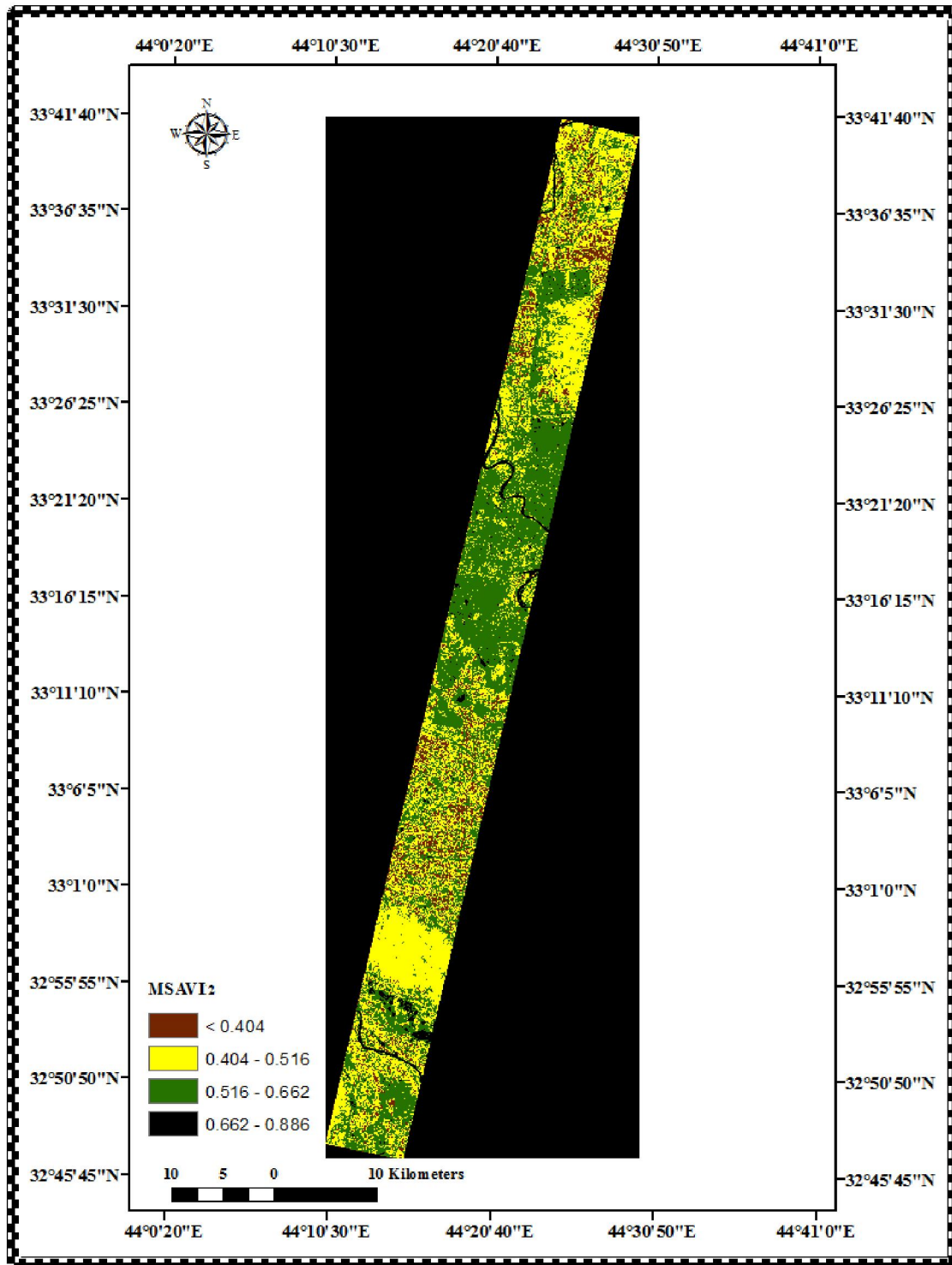


Figure 7. MSAVI<sub>2</sub> map of the study area.

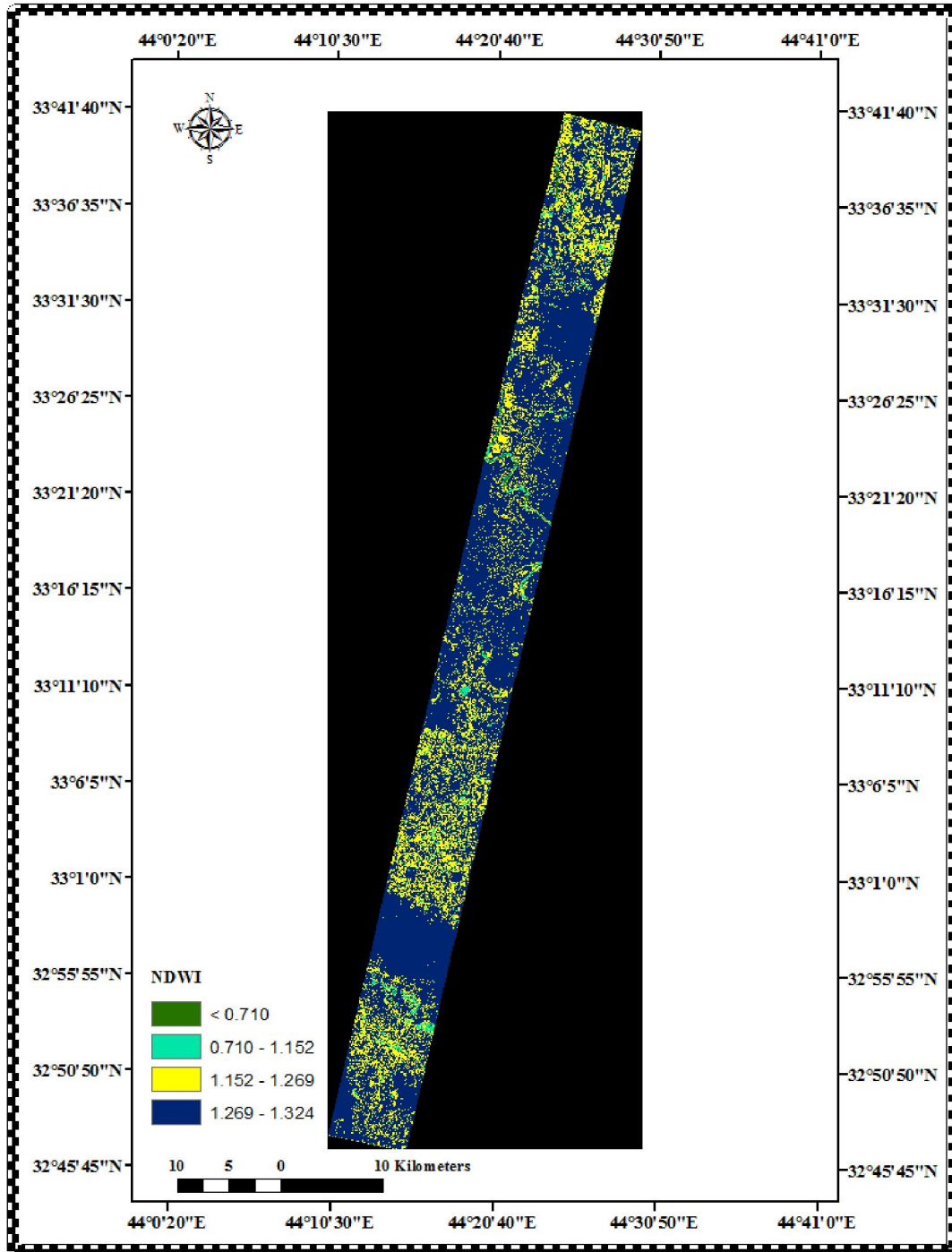


Figure 8. NDWI map of the study area.

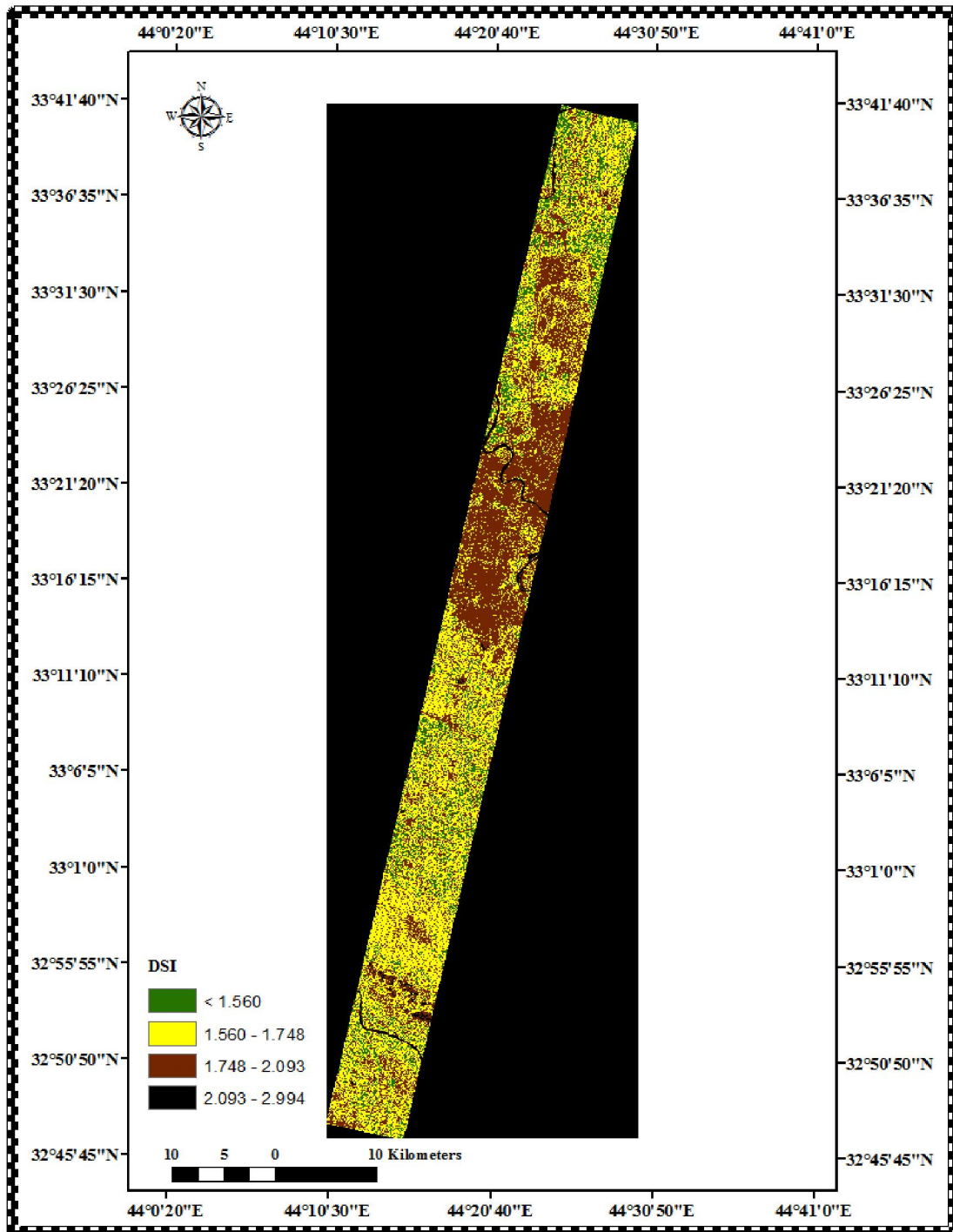


Figure 9. DSI map of the study area.

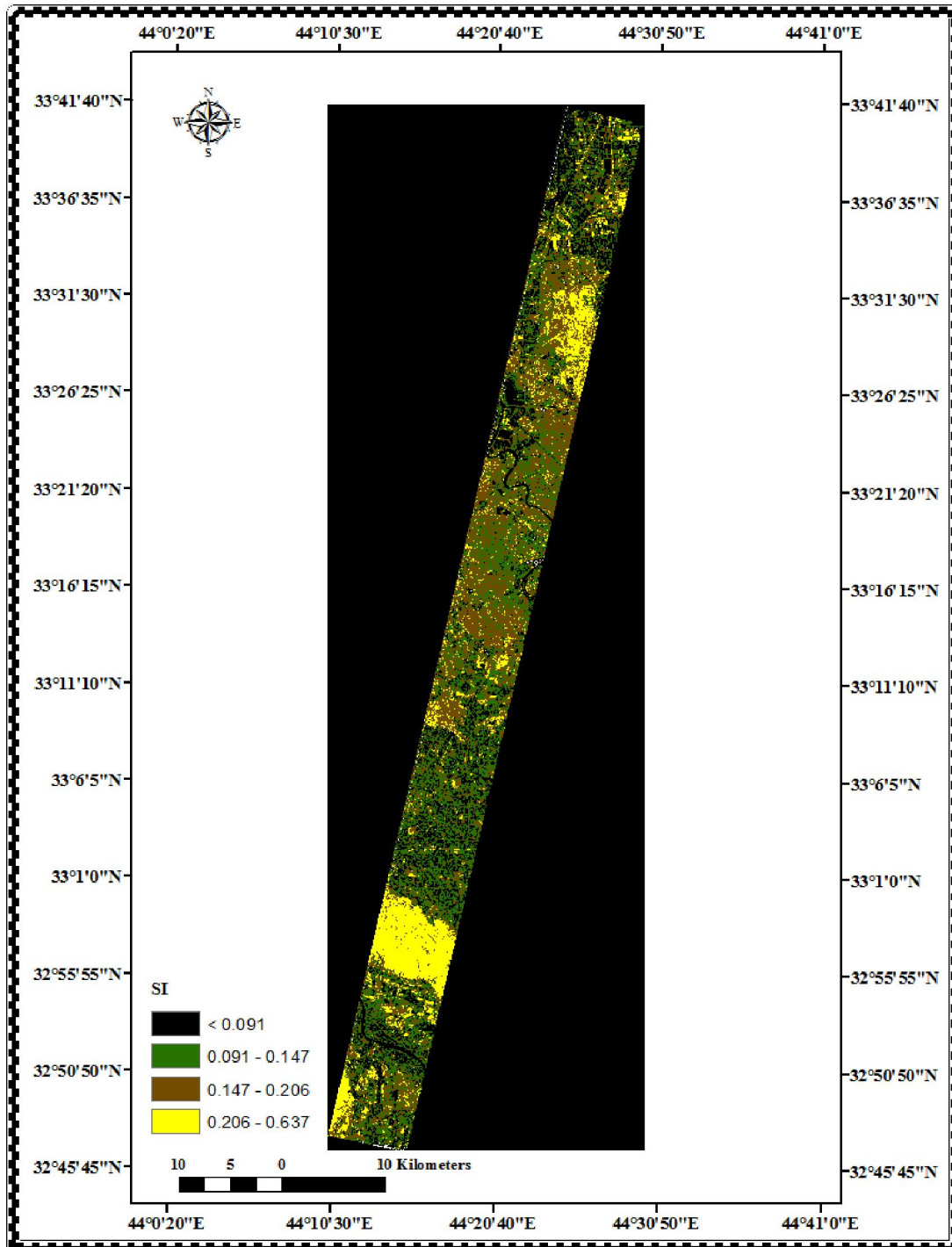


Figure 10. SI map of the study area.

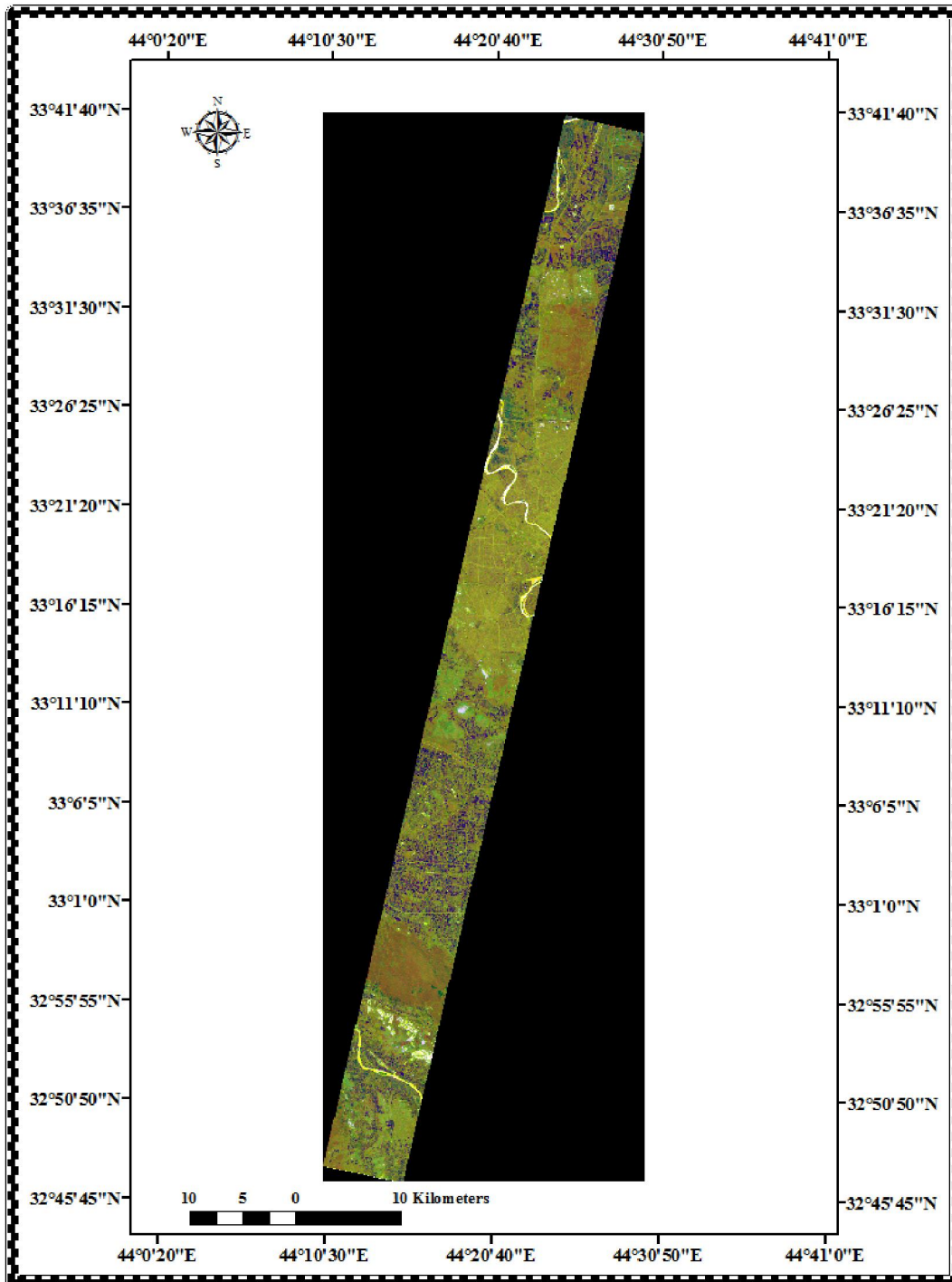


Figure 11. Multiple band image.

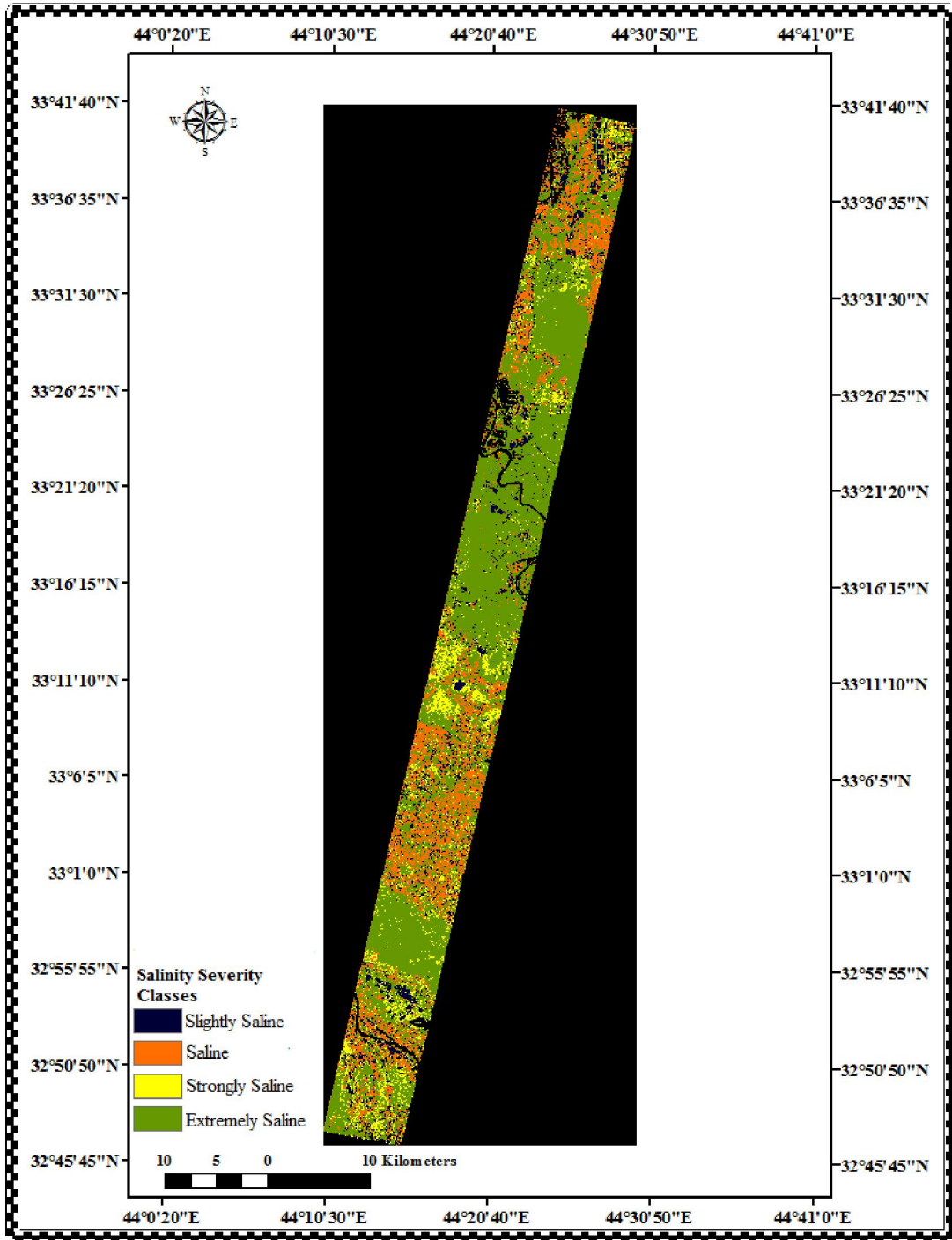


Figure 12. Soil salinity severity map of the study area.

**Table 5. Accuracy assessment of soil salinity severity classification using SVM.**

Class Name	Reference Totals	Classified Totals	Number Correct	Producers Accuracy	Users Accuracy
Slightly Saline	45	45	40	88.89%	88.89%

**Overall Classification Accuracy = 88.33%**

**Overall Kappa Statistics = 0.8444**

The four hyperspectral indices were combined with new multiple band image in ENVI software and used for classification using SVM (Fig. 11, 12). The study area was classified into four salinity severity classes i.e., slightly saline, saline, strongly saline, extremely saline. The region of interests (ROIs) was selected based on the data generated by 180 soil sampling. Classification probability threshold value set the probability that is required for the classifier to classify a pixel. Pixels where all rule probabilities are less than this threshold are unclassified. Here the value is set as 0, thus classifying all the pixels into one or the other class.

The major reasons for increasing soil salinity problems in the study area are intensive irrigation, rising groundwater table and consequent soil salinization are long-term problems for the central and southern Iraq. The genesis of soil salinity in the study area is attributed to the salt content of the irrigation water and salt contents of groundwater. Large scale salt accumulation is the result of low rainfall and high evapotranspiration caused by the arid climate. Insufficient and inappropriate drainage facilities for the disposal of saline drainage water generated by irrigated agriculture. Moreover Iraqi soils are rich in the naturally occurring parent materials such as limestone, sandstones (Qureshi and Falahi, 2015).

To evaluate the performance of SVM classification, a stratified random sampling method was used for accuracy assessment (Congalton, 1991). Table (5) summarizes the accuracy assessment of various salinity classes using SVM classification. The overall classification accuracy obtained was 88.33% with a kappa statistic of 0.8444. we found high accuracies for all salinity classes. The overall result showed that the SVMs are based on the principle called Structural Risk Minimization (SRM) maximizing the margin between a separating hyperplane and data points closest to the hyperplane (Huang et al., 2002).

#### 4. Discussions

Soil salinity, either naturally occurring or human-induced, is a serious global environmental problem, especially in arid and semi-arid regions. Soil

salinity was assessed with hyperspectral remote sensing so as to explore its potential application in this study area. The hyperspectral indices MSAVI2, NDWI, DSI, and SI were used as appraisal factors for assessing and mapping soil salinity. The results showed that these spectral indices are effective in distinguishing between various categories of salt affected soils. These indices when used for mapping of soil salinity severity using SVM method yielded maps of considerable accuracy with an overall accuracy of 88.33%. The validation of the accuracy assessment shows that soil salinity severity class maps are reliable and correlate significantly with actual field circumstances throughout the study area. Monitoring and temporal soil salinity investigation are the keystone exercise required for adequate natural resources management plans in the near future.

#### References

1. Khan, TO. Soil degradation, conservation and remediation. Springer Dordrecht Heidelberg, New York, London, 2014.
2. Allbed A, Kumar L. Soil salinity mapping and monitoring in arid and semi-arid regions using remote sensing technology: A review. *Advances in Remote Sensing* 2013;2(4):385-373.
3. Wu T-F, Lin C-J, Weng R C. Probability estimates for multi-class classification by pairwise coupling. *Journal of Machine Learning Research* 2004;5:1005-975.
4. Brugge, R. World weather news, August 2011. Department of Meteorology, University of Reading. Archived from the original on 29 June 2014.
5. Goodenough DG, Dyk A, Niemann KO, Pearlman JS, Chen H, Han T, Murdoch M, West C. Processing Hyperion and ALI for forest classification. *IEEE Transactions on Geoscience and Remote Sensing* 2003;41(6): 1331-1321.
6. ENVI.. Atmospheric Correction Module: QUAC and FLAASH User's Guide. Copyright © ITT Visual Information Solutions. Version 4.7, August, Edition 2009.
7. Liao LB, Jarecke PJ, Gleichauf DA, Hedman TR. Performance characterization of the

- hyperion imaging spectrometer instrument. Proc. of SPIE 2000;4135:275-264.
8. Thenkabail PS, Enclona EA, Ashton MS, Van Der Meer B. Accuracy assessments of hyperspectral waveband performance for vegetation analysis applications. *Remote Sensing of Environment* 2004a;91(3-4):376-354.
  9. Thenkabail PS, Enclona EA.; Ashton MS, Legg C, Dieu MJD. Hyperion, IKONOS, ALI. and ETM+ sensors in the study of African rainforests. *Remote Sensing of Environment* 20004b;90:43-23.
  10. Shaw R. Estimation of the electrical conductivity of saturation extracts from the electrical conductivity of 1:5 soil: water suspensions and various soil properties. Project Report Series QO94025, Department of Primary Industries, Queensland, Australia, 1994.
  11. Qi J, Chehbouni A, Huete AR, Kerr YH, Sorooshian S. A modified soil adjusted vegetation index. *Remote Sensing of Environment* 1994;48(2):126-119.
  12. Gao, B-C. NDWI - A normalized difference water index for remote sensing of vegetation liquid water from space. *Remote Sensing of Environment* 1996;58(3):266-257.
  13. Wu J, Liu Y, Wang J, He T. Application of Hyperion Data to land degradation mapping in the Hengshan region of China. *International Journal of Remote Sensing* 2010;31(19):5161-5145.
  14. Khan NM, Rastoskuev VV, Shalina EV, Sato Y. Mapping Salt-affected soils using remote sensing indicators - A Simple Approach with the use of GIS IDRISI. 22nd Asian Conference on Remote Sensing, 5-9 November 2001, Copyright (c) 2001 Centre for Remote Imaging, Sensing and Processing (CRISP), National University of Singapore 2001.
  15. Hsu C-W, Chang C-C, Lin C-J. A practical guide to support vector classification. Department of Computer Science, National Taiwan University 2003.
  16. Tilley DR, Ahmed M, Son JH, Badrinarayanan H. Hyperspectral reflectance response of freshwater macrophytes to salinity in a brackish subtropical marsh. *Journal of Environmental Quality* 2007;36(3):789-780.
  17. Carter GA. Responses of leaf spectral reflectance to plant stress. *American Journal of Botany* 1993;80(3):243-239.
  18. Yang, JY, Zheng W, Tian Y, Wu Y, Zhou DW. Effects of various mixed salt-alkaline stresses on growth, photosynthesis, and photosynthetic pigment concentrations of *Medicago ruthenica* seedlings. *Photosynthetica* 2011;49(2):284-275.
  19. Elhag M. Evaluation of different soil salinity mapping using remote sensing techniques in arid ecosystems, Saudi Arabia. *Journal of Sensors* 2016; Article ID 7596175, 8 pages.
  20. Singh RP, Sirohi A. Spectral reflectance properties of different types of soil surfaces. *ISPRS Journal of Photogrammetry and Remote Sensing* 1994;49(4):40-34.
  21. Fernandez-Buces N, Siebe C, Cram S, Palacio JL. Mapping soil salinity using a combined spectral response index for bare soil and vegetation: A Case Study in the Former Lake Texcoco, Mexico. *Journal of Arid Environments* 2006;65(4):667-644.
  22. Qureshi AS, Al-Falahi AA. Extent, characterization and causes of soil salinity in central and southern Iraq and possible reclamation strategies. *Journal of Engineering Research and Applications* 2015;5(1):94-84.
  23. Congalton RG, A review of assessing the accuracy of classifications of remotely sensed data. *Remote Sensing of Environment* 1991;37(1):46-35.
  24. Huang C, Davis LS, Townshend JRG.. An assessment of support vector machines for land cover classification. *International Journal of Remote Sensing* 2002;23(4):749-725.

11/11/2017